Laser Cooling Under Ambient Conditions in Yb^{3+}:KYW

Laura B. Andre*[a], Long Cheng[a], Alexander J. Salkeld[a], Luis H. C. Andrade[b], Sandro M. Lima[b], Junior R. Silva[b], Stephen C. Rand[a,c]

[a]EECS Department, University of Michigan, 1301 Beal Ave., Ann Arbor, MI, USA 48109-2122; [b]Programa em Recursos Naturais, Universidade Estadual de Mato Grosso do Sul, Dourados, Brazil 79804-970; [c]Department of Physics, University of Michigan, 450 Church Street, Ann Arbor, MI, USA 48109-1040

ABSTRACT

We report the first observation of laser cooling in 1%Yb^{3+}:KYW and discuss factors that limit the cooling efficiency. Cooling by 10 K from room temperature at atmospheric pressure was achieved in this crystal at a wavelength of 1025 nm using 8 W from a seeded fiber amplifier. The temperature of the sample was measured using a calibrated differential luminescence thermometry method and was verified with a thermal camera. Infrared imagery and 3-D modeling were used to analyze the impact of thermal conduction, thermal convection, black-body radiation, and background impurities. The simulated results agree with experimental measurements confirming that the chief limitation of laser cooling at room temperature and atmospheric pressure is thermal conduction from sample supports. Best results were obtained for samples mounted on silica aerogel. Theoretical improvement of cooling efficiency in vacuum by exploiting impurity absorption saturation is also discussed.

Keywords: Optical Refrigeration, Ytterbium, Absorption, Laser Applications, Ions, Crystals, Luminescence, Phonons

1. INTRODUCTION

The use of light for optical refrigeration began with the pioneering experiments of Epstein et al. based on laser-induced anti-Stokes fluorescence in Yb^{3+}:ZBLANP glass which achieved net cooling of approximately 1 Kelvin/Watt in 1995.[1] The successful outcome vindicated an early suggestion by Pringsheim[2] that optical interactions could cool bulk matter and confirmed the thermodynamic analysis by Landau[3] which showed that changes in the mode structure or entropy of electromagnetic fields could account for entropy flow and heat transfer quantitatively. Over the next two decades, advances in experimental methods and the purification of materials led to cooling of crystalline media,[4] the reduction of minimum attainable temperatures to the cryogenic range,[5,6] demonstration of the first optical cryocooler,[7] and emergence of the concept of self-cooling or radiation-balanced lasers (RBL).[8,9] Despite these advances, only one active ion has been investigated for lasers with reduced heat loads, namely trivalent Ytterbium, and the host media of self-cooled lasers reported to date comprise only KGW,[9] YLF,[10] and YAG.[10,11] Consequently, the field is still at an early stage. In this paper, we demonstrate for the first time laser cooling of Yb:KYW which has a high figure of merit for radiation-balanced lasing.

In past work, laser cooling by 8.8 K of an Yb:YAG crystal was reported at atmospheric pressure inside a sealed chamber.[11] For deep cooling experiments, special enclosures are required to reduce the substantial heat load imposed on the sample by blackbody radiation from the environment.[1] On the other hand for self-cooling laser experiments the objective is to operate under ambient pressure and temperature, maintaining the gain medium in equilibrium with the environment at room temperature. In the latter situation the blackbody heat load, proportional to the difference between sample and lab temperature,[1] is vanishingly small and thermal conduction through the sample support structure can be anticipated to be the limiting factor in heat transport. Provision of a support that aids laser cooling by minimizing thermal conduction but is nevertheless rigid is therefore an important aspect of the design of practical RBL resonators. Hence we compared the use of various sample support materials and found that aerogel improved the cooling power by an order of magnitude with respect to that of glass while maintaining an open, rigid structure suitable for high power self-cooled laser designs. This finding is expected to be vital for future attainment of radiation-balanced conditions in Yb:KYW, since current commercially-available crystals have impurity concentrations that are nearly high enough to prevent cooling altogether.

*lbandre@umich.edu; phone: 1 734 764-9578; https://dynamo.engin.umich.edu

2. METHODS

2.1 Setup and Yb:YAG validation experiment

For the present experiments, a tunable single-mode Ti:Sapphire laser (M-Squared) was used to seed an Yb fiber amplifier (IPG Photonics YAR-10K-1030-LP-SF) capable of delivering up to 11 Watts continuous-wave in the wavelength range 1020-1040 nm. The output of the amplifier was focused with a 20 cm lens into Brewster-cut samples of 3%Yb:YAG (Scientific Materials) and 1%Yb:KYW (Altechna), both with dimensions of 1×1×10 mm^3. The Yb:YAG crystal is included in this paper as a point of reference and for validation of experimental methods. The pump laser made a single pass through the sample and the infrared luminescence was collected with a multimode optical fiber (Ocean Optics QP600-2-VIS-NIR) of 0.4 NA connected to a 0.5 m grating spectrometer (Oriel 74100) equipped with a CCD detector (Andor DU491A-1.7). The absorption cross section was calculated by the McCumber relation[12] using the corrected fluorescence data. The absorption coefficient of the crystal at 1030 nm is measured by tuning the Ti:Sapphire laser to that wavelength and measuring the power before and after the crystal to scale the absolute value of absorption and emission coefficients shown in Figure 1(a). The dashed vertical line indicates the calculated mean fluorescence wavelength, which agrees with recent published values.[11] The sample temperature is monitored using differential luminescence thermometry (DLT)[13] which deduces the temperature through the variations of the fluorescence lineshape. The DLT signals were measured in the spectral range 960-975 nm for Yb:YAG and were calibrated by direct heating or cooling of the sample using a temperature controller (Quantum Northwest Flash 300) with an accuracy of ±0.01 K. For each temperature point in the calibration, the pump beam is introduced in the sample and the DLT signal is measured, giving the linear relation plotted in Figure 1(b).

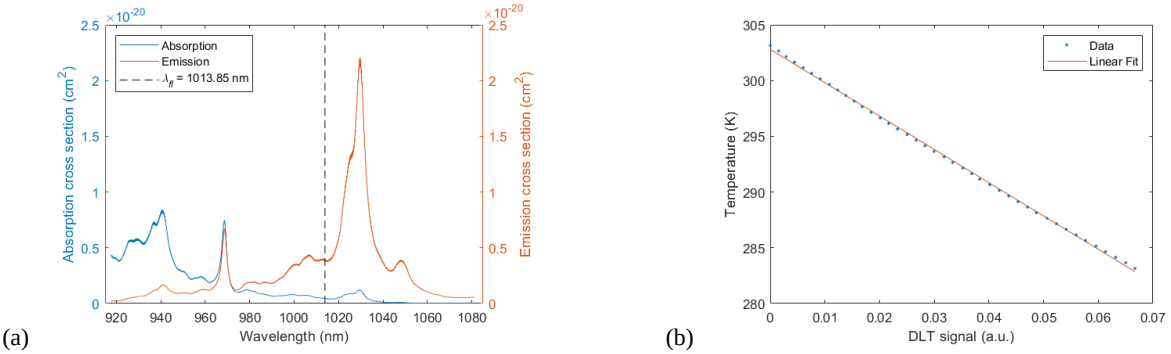

Figure 1. (a) Corrected absorption and emission cross sections for Yb:YAG. The dashed vertical line indicates the mean fluorescent wavelength, λ_{fl}. (b) DLT calibration data points for Yb:YAG and linear fit: T = -298.839×DLT+302.793 K.

The processing time for each temperature determination in the cooling experiments was short enough, about 2 seconds, to permit real-time tracking of the temperature dynamics. Pumping the Yb:YAG crystal at 1030 nm with 1 W pump power gives the temperature variation in time plotted in Figure 2(a). The temperature change of the sample was recorded at varying pump wavelengths and is shown in Figure 2(b). When pumping at longer wavelengths, the decrease of Yb^{3+} absorption will reduce the fluorescence intensity and leads to larger error bars at wavelengths greater than 1040 nm.

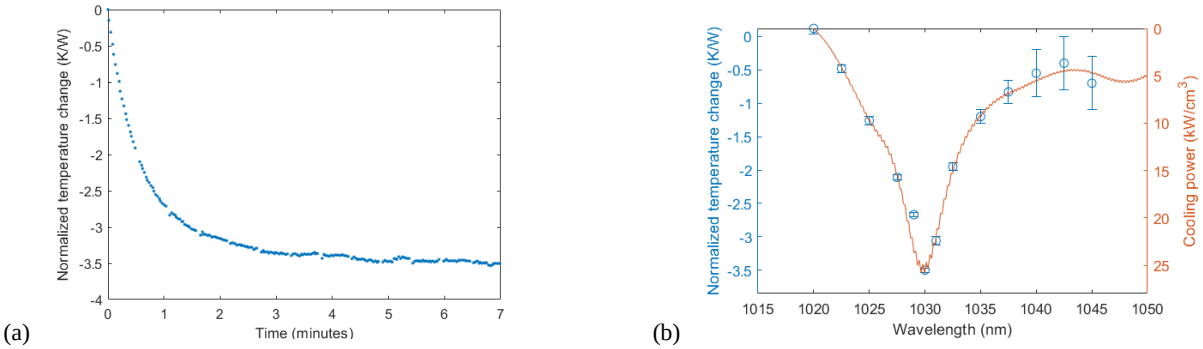

Figure 2. (a) Temperature change in K/W versus time of Yb:YAG when pumped at 1030 nm with 1 W. (b) Plot of wavelength versus normalized temperature change and cooling power fit with η_{ext} = 0.9950±0.0109 and α_b = (1.6±0.26)×10^{-4} cm^{-1}. Noise oscillations in theoretical curve arise because of dependence on spectral data.

2.2 Yb:KYW spectroscopy

The procedure outlined in Section 2.1 was used to test the 1%Yb:KYW sample. The crystal is anisotropic with orthogonal crystalooptic axes N_m, N_p, and N_g. The sample is N_p-cut with Brewster angle ends designed for 998 nm with E||N_m. The fluorescence was collected with the same multimode fiber optic system used in the Yb:YAG experiments. The fiber was oriented parallel to the N_m axis, and a wire grid polarizing film (Edmund Optics, 400-1200 nm) was placed between the crystal and fiber to maintain the polarization of collected fluorescence along the N_m crystal axis. Again, the McCumber relation was used to determine absorption cross section, and plots of the emission and absorption for E||N_m may be found in Figure 3(a). For Yb:KYW, DLT was used to track the width of the feature between 970-990 nm and the change in temperature at various pump wavelengths was measured, as shown in Figure 3(b). The optimum cooling wavelength determined experimentally was ~1025 nm, in close accord with the theoretical temperature minimum at 1023 nm.

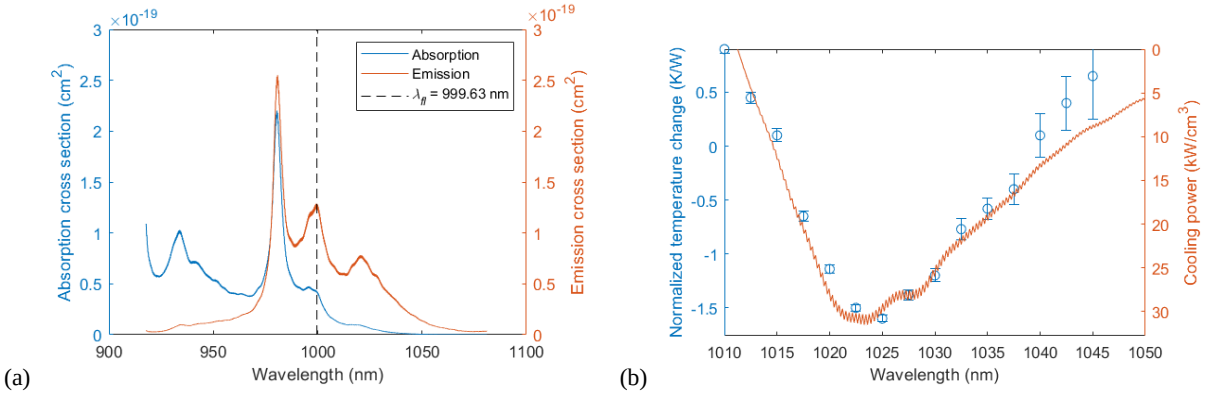

Figure 3. (a) Corrected absorption and emission cross sections for Yb:KYW for E||N_m. The dashed vertical line indicates the mean fluorescent wavelength, λ_{fl}. (b) Plot of wavelength versus normalized temperature change and cooling power fit with η_{ext} = 0.9815±0.0114 and α_b = (2.10±0.31)×10^{-3} cm^{-1}. Noise oscillations in theoretical curve arise from use of spectral data.

2.3 Estimation of η_{ext} and α_b

Temperature changes due to Anti-Stokes Fluorescent (ASF) emission at various pump wavelengths are shown in Figure 3(b). A best fit was obtained to the expression for cooling power[11], namely

$$\frac{P_c}{V} = \left(\eta_{ext}\frac{\lambda}{\lambda_{fl}} - 1\right)\alpha_c(\lambda)I_0, \tag{1}$$

using the absorption coefficient $\alpha_c(\lambda)$ of the cooling ion and mean fluorescent wavelength λ_{fl} from the corrected spectra in Figure 3(a). With external quantum efficiency η_{ext} as the fitting parameter, the red curve of Figure 3(b) was obtained with a best fit value of η_{ext} = 0.9815±0.0114. The background absorption coefficient was estimated by setting the cooling power equal to the heating due to impurity absorption at the point where the temperature change is zero, $P_c(\Delta T{=}0) = \alpha_b P_0 L$. In this way the background absorption coefficient was determined to be (2.10±0.31)×10^{-3} cm^{-1} in the Yb:KYW sample.

Thermal lens spectroscopy (TLS) was also performed on the sample as a means of independent determination of external quantum efficiency and background impurity absorption. Experimentally, a tunable Ti:Sapphire laser was used to pump the samples and a HeNe laser beam was used to probe the induced thermal lens at 632.8 nm. In order to increase the signal-to-noise ratio, the pump beam was chopped mechanically and the signal from the photodiode was detected synchronously using a lock-in amplifier. The TLS signal was modeled by considering two separate lensing effects – the fast photoinduced population change between the ground and excited states, and a slower thermal diffusion component. The refractive index changes due to both processes had to be included to model the complex transient TLS signal accurately.[14] The experiment was performed with pump wavelengths ranging from 932 nm to 1030 nm. The normalized TLS signal and the fits accounting for the two effects are shown in Figure 4(a). At 942 nm, a strong population lens effect caused a rapid initial increase of the signal. At later times, the thermal effect dominated the signal, causing it to decrease. With the pump tuned to 1025 nm, the thermal component in Figure 4(a) reversed sign, indicative of sample cooling. The fit of the TLS signal at

each pump wavelength provided a value for the thermal lens strength, and the cooling efficiency derived from it. It was then possible to plot and fit cooling efficiency versus wavelength based on the TLS data using the expression[1,14]

$$\eta_c = \eta_{ext}\left(\frac{\alpha_c(\lambda)}{\alpha_c(\lambda)+\alpha_b}\right)\frac{\lambda}{\lambda_{fl}} - 1. \quad (2)$$

This fitting procedure gave values of η_{ext} = 0.996±0.007 and α_b = (1.3±0.2)×10^{-3} cm^{-1} for Yb:KYW, which are in close agreement with those determined by the DLT method. In an Yb:YAG sample from Scientific Materials, the same approaches yielded η_{ext} = 0.9950±0.0109 and α_b = (1.6±0.26)×10^{-4} cm^{-1} using the DLT method and η_{ext} = 0.983±0.007 and α_b = (2.3±0.7)×10^{-3} cm^{-1} using the TLS technique.

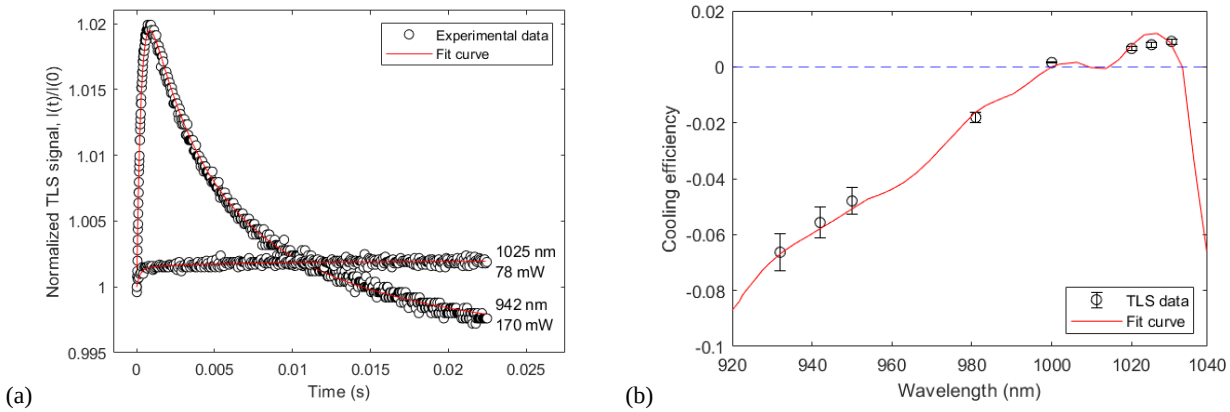

Figure 4. (a) TLS transient signals for Yb:KYW at 942 nm (heating) and 1025 nm (cooling) amplified by almost 7 times. (b) TLS measurements of cooling efficiency in Yb:KYW as a function of wavelength. The values of η_{ext} = 0.996±0.007 and α_b = (1.3±0.2)×10^{-3} cm^{-1} are obtained by the best fit of Eq. (2) to the data.

2.4 Impurity absorption saturation and minimum achievable temperature

To date, possible variations of background impurity absorption with wavelength, temperature, or intensity have not been taken into account in analyses of laser cooling. Current theory assumes that α_b is purely a constant. Here we consider theoretical consequences of intensity dependence of absorption by the cooling ion $\alpha_c(I)$ and by background impurities $\alpha_b(I)$ to show that saturation effects can significantly affect the minimum achievable temperature (MAT) in ASF cooling. The MAT can be found by setting the cooling efficiency equal to zero and solving for temperature:

$$T_{min} = \left(\frac{\hbar\Omega}{k_B}\right) / \log_e\left\{1 + \left(\eta_{ext}\left(\frac{\nu_{fl}}{\nu}\right) - 1\right)\frac{\alpha_c(I)}{\alpha_b(I)}\left[\exp(\hbar\Omega/k_B T_0) - 1\right]\right\}. \quad (3)$$

We assumed that the intensity dependence of absorption follows the standard model: $\alpha_{c,b}(I) = \alpha_{b,c}(0)/(1+I/I_{c,b})$, where $I_{c,b}$ are the saturation intensities of the cooling ion and background respectively. Figure 5 was then prepared to display the effect of impurity absorption saturation on cooling in Yb:KYW. If $I_b \gg I_c$, the cooling power saturates before the background absorption does, so that the MAT increases with increasing pump intensity. When $I_b = I_c$ there is no dependence of net cooling on intensity. However, if $I_b < I_c$, the MAT drops substantially with increasing pump intensity. These three cases are presented graphically in Figure 5(a). Using the absorption spectrum of Yb:KYW, the values of η_{ext} and $\alpha_b(0)$ obtained from the DLT estimate, and I_c/I_b = 5 in equation (3), the MAT achievable in vacuum at various wavelengths was calculated for two representative input intensities and plotted in Figure 5(b). By comparing the two curves for T_{min}, it is evident that lower temperatures can be reached in ASF cooling at high intensities when impurity absorption saturates before the absorption of the coolant ions.

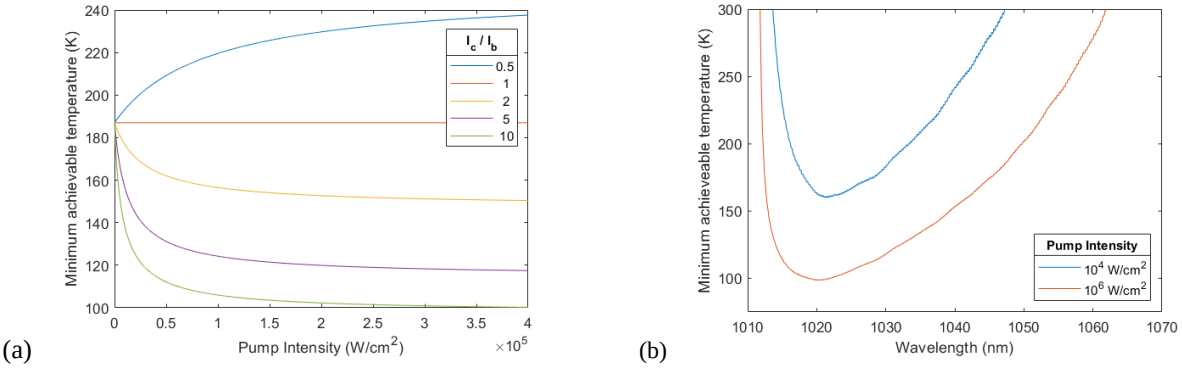

Figure 5. Simulation of minimum achievable temperatures based on Eq. (3) in Yb:KYW. (a) MAT versus pump intensity for different ratios of the Yb^{3+} saturation intensity to background saturation intensity assuming I_c = 10^5 W/cm^2 at a pump wavelength of 1025 nm. (b) MAT versus wavelength assuming I_c/I_b = 5 and I_c = 10^5 W/cm^2.

3. EXPERIMENTAL RESULTS

3.1 Thermal camera measurements

In addition to DLT, a thermal camera (FLIR A655sc) was used to verify the exact temperature values being measured and evaluate the thermal conduction from the sample support. For each crystal, a calibration was performed using the afore-mentioned temperature controller. The temperature of the crystal was varied from 10-50 °C and the surface emissivity was calculated by relating the set crystal temperature to the infrared radiation received by the camera. In this way, we were able to determine the emissivity of each crystal as a function of temperature and determine absolute temperature measurements from the thermal camera during cooling experiments. In initial experiments, the samples were supported by three glass capillary tubes. Figure 6(a),(b) shows the thermal camera image before and after pumping Yb:KYW with 1 W at 1025 nm. The fiber used to collect fluorescence for the DLT measurement can be seen near the top of the image. In Figure 6(b), with the pump on, tuned to the long wavelength tail of the absorption, the crystal became darker indicating a reduction of temperature. Transient temperatures were also recorded by specifying areas of interest in the camera software and averaging over the pixels in that area. Figure 6(c) shows the temperature over time of crystal (blue) and glass supports (red) using the thermal camera. It should be noted that the temperature of the sample support was not calibrated and can

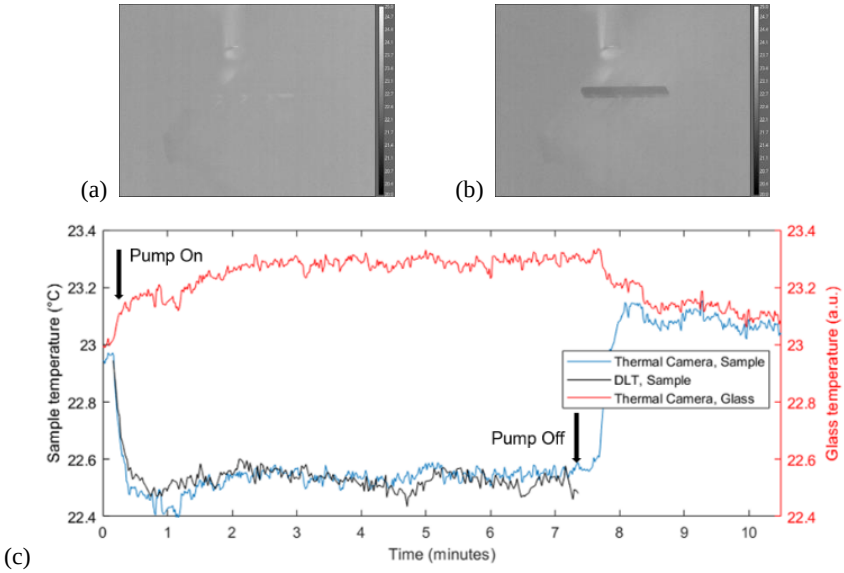

Figure 6. Thermal camera image of Yb:KYW on glass supports with the pump (a) off and (b) on. (c) Temperature versus time comparing DLT and thermal camera measurements for glass supports.

only reliably indicate relative measurements in these plots. The temperature recorded using DLT (black) is plotted for comparison, and the absolute temperatures from the various methods were in close agreement. Despite the 0.5 K temperature drop achieved, the curves in Figure 6(c) indicate a poor choice of sample support. With the pump on, the temperature of the glass supports increases even though the sample is being cooled. We hypothesize that this is due to the glass absorbing some of the fluorescence emitted from the crystal. Additionally, the temperature of the sample dropped when the pump was initially turned on, but subsequently increased with time. This behavior could be interpreted as the result of fast cooling in the interaction volume followed by an influx of heat from uncooled portions of the sample itself or heat influx through contacts between the sample and its support. At about 7.5 minutes, the pump was turned off. At this point, fluorescence emission stopped so the DLT measurement ended, and the temperatures of the sample and glass support returned to equilibrium. The temperature of the glass slowly decreased, and the temperature of the crystal rapidly increased to a point above its initial temperature because of heating through thermal conduction by the glass supports.

To address this issue, the glass supports were replaced by a silica aerogel disk (BuyAerogel.com). Thermal camera images with the (1 Watt) pump off and on again at 1025 nm are shown in Figure 7(a),(b). Pumping the crystal at 1025 nm with the aerogel support resulted in an even darker thermal image of the crystal, indicating the sample support improved the cooling of the crystal. The transient temperature signals plotted in Figure 7(c) confirm the temperature of the crystal dropped by about 1.8 K. The temperature of both the crystal and the aerogel dropped with the pump on, indicating that there was no heating of the sample support. Further, the respective equilibrium temperatures returned to their initial values. Consequently, despite the increase in contact area with the aerogel, the cooling efficiency improved by over an order of magnitude due to the reduced thermal conductivity of the aerogel as a sample support.

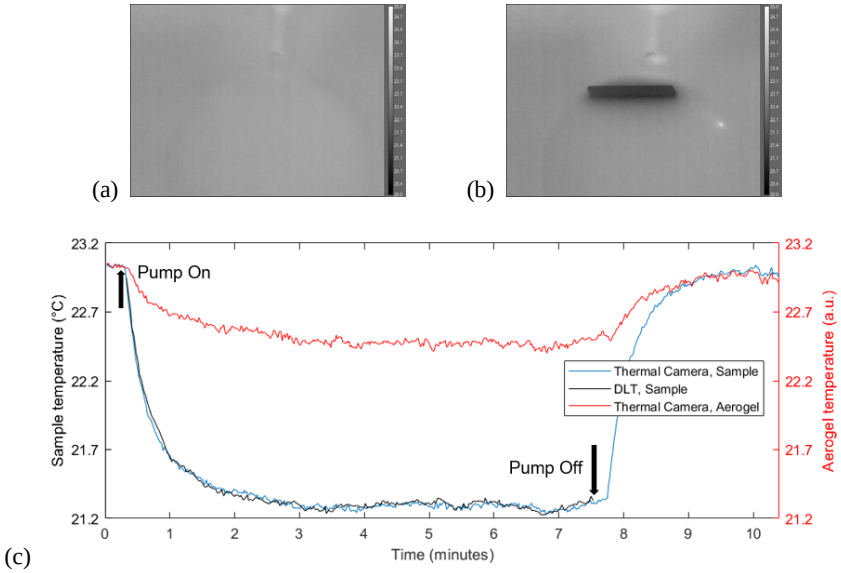

Figure 7. Thermal camera image of Yb:KYW on aerogel support with the pump (a) off and (b) on. (c) Temperature versus time comparing DLT and thermal camera measurements for aerogel support.

3.2 COMSOL model

3-D COMSOL simulations of heat diffusion and cooling were used to confirm the insights gained from the thermal camera measurements and to investigate factors limiting cooling efficiency. The model included the effects of thermal conduction from sample support, thermal convection from air, optical cooling, and black body radiation. Figure 8 shows the simulation results for both the glass capillary tubes (a) and silica aerogel (b) as sample supports resting on a glass slide in air. The model gives 0.44 K and 1.89 K temperature drops pumping with 1 W at 1025 nm for the glass and aerogel, respectively. The simulated change in temperature achieved with each sample support is in close agreement with the experimental data collected by DLT and the thermal camera. Aerogel has an extremely low thermal conductivity and is therefore able to maintain a large temperature gradient and minimize the heat flow between the crystal and glass slide mount. Additionally, the surface emissivity of silica aerogel is much smaller than glass, which reduces the energy incident on the crystal from black body radiation. Aerogel is clearly a superior choice over glass for sample support.

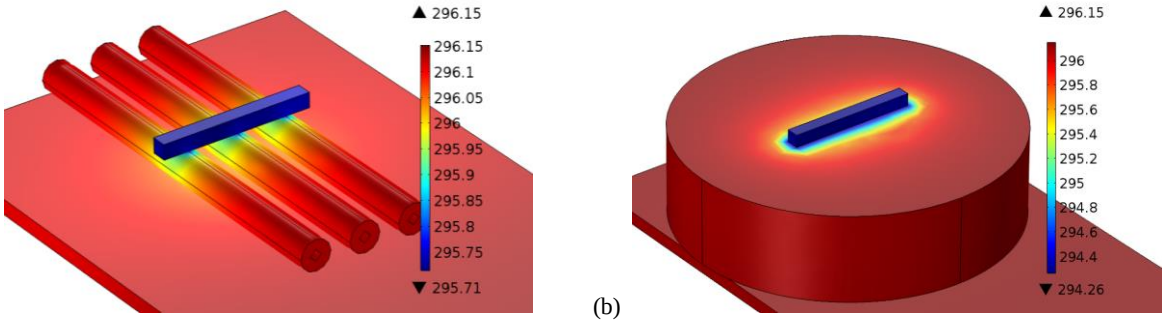

Figure 8. COMSOL simulation results for (a) glass capillary tubes and (b) silica aerogel structures supporting a 1×1×10 mm^3 crystal of Yb:KYW and using η_{ext} = 0.983.

4. CONCLUSIONS

We validated characterization tools for laser cooling in 3%Yb:YAG samples under ambient conditions and applied them to demonstrate record cooling of 3.5K/W in Yb:YAG in air and to cool a crystal of 1%Yb:KYW for the first time. The external quantum efficiency and background impurity absorption, estimated using DLT and TLS measurements, were in excellent agreement. Temperature measurements performed with the thermal camera and COMSOL simulations confirmed that aerogel is superior to glass for the purpose of providing rigid sample support in cooling or RBL experiments. An expression for minimum achievable temperature (MAT) that included the intensity dependence of absorption by coolant and impurity ions was developed and analyzed. Substantial reductions of the MAT were predicted to be attainable at intensities above the impurity saturation intensity, provided the saturation intensity of the coolant ions in turn exceeds that of the impurities ($I_b < I_c$). Thus, saturation can in principle exercise a profound effect on MAT in laser cooling of solids by the ASF technique.

Acknowledgements: This research was supported by a Multidisciplinary University Research Initiative sponsored by the Air Force Office of Scientific Research, grant FA9550-16-1-0383.

REFERENCES

[1] Epstein, R. I., Buchwald, M. I., Edwards, B. C., Gosnell, T. R. and Mungan, C. E., "Observation of laser-induced fluorescent cooling of a solid," Nature 377, 500-503 (1995).
[2] Pringsheim, P. Z., "Zwei Bemerkungen uber den unterschied von luminescenz- und temperaturstrahlung," Z. Phys. 57, 739-746 (1929).
[3] Landau, L. ,"On the thermodynamics of photoluminescence," J. Phys. (Moscow) 10, 503-506 (1946).
[4] Bowman, S. R. and Mungan, C. E., "New materials for optical cooling," Appl. Phys. B 71, 807-811 (2000).
[5] Melgaard, S. D., Seletskiy, D. V., Lieto, A. D., Tonelli, M. and Sheik-Bahae, M., "Optical Refrigeration to 119K, below National Institute of Standards and Technology cryogenic temperature," Opt. Lett. 38, 1588-1590 (2013).
[6] Melgaard, S. D., Albrecht, A. R., Hehlen, M. P. and Sheik-Bahae, M., "Solid-state optical refrigeration to sub-100 Kelvin regime," Sci. Rep. 6, 20380 (2016).
[7] Hehlen, M. P., Meng, J., Albrecht, A. R., Lee, E. R., Gragossian, A., Love, S. P., Hamilton, C. E., Epstein, R. I. and Sheik-Bahae, M., "First demonstration of an all-solid-state optical cryocooler," Light: Science & Applications 10, 1038 (2018).
[8] Bowman, S. R., "Lasers without internal heat generation," IEEE J. Quantum Elect. 35, 115-122 (1999).
[9] Bowman, S. R., O'Connor, S. P. and Biswal, S., "Ytterbium laser with reduced thermal loading," IEEE J. Quantum Elect. 41, 1510-1517 (2005).
[10] Yang, Z., Albrecht, A. R., Meng, J. and Sheik-Bahae, M., "Radiation balanced thin disk lasers," CLEO: Science and Innovations, Optical Society of America, paper SM4N.5 (2018).
[11] Filho, E. S., Nemova, G., Loranger, S. and Kashyap, R., "Laser-induced cooling of a Yb:YAG crystal in air at atmospheric pressure," Opt. Express 21, 24711-24720 (2013).
[12] McCumber, D. E., "Einstein relations connecting broadband emission and absorption spectra," Phys. Rev. 136.4A, A954-A957 (1964).

[13] Seletskiy, D. V., Hasselbeck, M. P., Sheik-Bahae, M. and Epstein, R. I., "Fast differential luminescence thermometry," Proc. SPIE 7228, 72280K (2009).
[14] Silva, J. R., Malacarne, L. C., Baesso, M. L., Lima, S. M., Andrade, L. H. C., Jacinto, C., Hehlen, M. P. and Astrath, N. G. C., "Modeling the population lens effect in thermal lens spectrometry," Opt. Lett. 38, 422-424 (2013).